J Mater Sci (2010) 45:2760–2769
DOI 10.1007/s10853-010-4263-4

Microstructure of high velocity oxy-fuel sprayed Ti_2AlC coatings

Marie Sonestedt · Jenny Frodelius · Jens-Petter Palmquist · Hans Högberg · Lars Hultman · Krystyna Stiller

Received: 31 August 2009 / Accepted: 22 January 2010 / Published online: 9 February 2010

Abstract The microstructure formation and phase transformations in Ti_2AlC-rich coatings deposited by High Velocity Oxy-fuel spraying of Maxthal 211® powders is presented. High resolution electron microscopy analysis, using both scanning and transmission electron microscopy with energy dispersive spectrometry and energy filtering, combined with X-ray diffraction reveals that the coatings consist of Ti_2AlC grains surrounded by regions of very small TiC grains embedded in Ti_xAl_y. The composition of the Ti_xAl_y depends on its surrounding and varies with size and distribution of the adjacent TiC grains. Impact of spray parameters on coating microstructure is also discussed. Two spray parameters were varied; powder size distribution and flame power. They were found to greatly affect the coating microstructure. Increasing powder size and decreasing flame power increase the amount of Ti_2AlC, but produces thinner coatings with lower cohesion. Larger powder size will also decrease oxygen incorporation.

Introduction

Ti_2AlC belongs to a group of ternary carbides named $M_{n+1}AX_n$ phases. These materials are interesting due to their combination of metallic and ceramic properties; they are, e.g. good thermal and electrical conductors, machinable and lightweight [1]. Ti_2AlC has good temperature and oxidation resistance [2–4], which make this material a possible candidate for use as a coating against high temperature oxidation. So far, Ti_2AlC bulk materials have been produced using, e.g. spark plasma sintering [5], and to produce thin films, e.g. PVD technique has been used [6, 7]. However, in order to fabricate coatings with a thickness of at least 100 μm another approach is necessary, and different thermal spray techniques have proven to be useful for various Ti-based materials systems [8, 9].

We have recently demonstrated that high velocity oxy-fuel (HVOF) spraying can be used to fabricate coatings from Ti_2AlC powder [10]. HVOF spraying is a thermal spray process based on the combustion of oxygen and a fuel gas. The high-energy exhaust flame heats and accelerates the powder particles to supersonic speed. This method is known to produce dense coatings with good adhesion to the substrate and with a relatively low amount of incorporated oxygen and maximum phase stability for carbides [11, 12]. However, we found using X-ray diffraction analysis that a significant fraction of the Ti_2AlC phase of the powder decomposes during HVOF processing. According to this analysis, besides Ti_2AlC, the coatings contained Ti_3AlC_2, TiC and Ti–Al phases. It also appeared that the decomposition of the original powder was dependent both on the total gas flow during spraying and upon powder size. But, this first study does not reveal the details of the Ti_2AlC phase decomposition during coating deposition and the influence of the spraying parameters was not studied carefully enough to allow for a more complete understanding of the processes behind the coating formation.

M. Sonestedt (✉) · K. Stiller
Microscopy and Microanalysis, Department of Applied Physics, Chalmers University of Technology, 412 96 Göteborg, Sweden
e-mail: marie.sonestedt@chalmers.se

J. Frodelius · H. Högberg · L. Hultman
Thin Film Physics Division, Department of Physics, Linköping University, IFM, 581 83 Linköping, Sweden

J.-P. Palmquist
Kanthal AB, 734 27 Hallstahammar, Sweden

Here, we present a study of the detailed microstructure and phase transformations in HVOF-spray deposited Ti_2AlC coatings as a function of process parameters. In order to retain a maximum of the Ti_2AlC phase in the coatings it is important to use a large-enough powder size and low enough gas flow. It is furthermore clear that thick coatings with good cohesion are produced only when the energy of the in-flight powder attains some critical level necessary for an efficient sticking. It is also shown that powder size affects oxygen content. Based on the high-resolution techniques applied for investigation of the coatings, the microstructure is compared to the previously proposed hypothesis [10] of the fate of Ti_2AlC powder during the spraying process.

Experimental

Fabrication of coatings

Coatings have been produced using three different gas flow rates and four different powder size distributions (XS, S, M and L). The used gas flow rates were 953 L/min (high), 703 L/min (medium) and 441 L/min (low). Table 1 lists the size distributions of the powder, which was crushed and sifted bulk Ti_2AlC, Maxthal 211®, from Kanthal AB, Sweden. More details about the powder can be found elsewhere [10].

All depositions were made on stainless steel substrates (60 × 19 × 1.5 mm, AMS 5604, US standard). Before spraying, the substrates were cleaned with acetone and manually grit blasted with alumina (grit 60 at 4 bar). They were mounted on a carousel rotating at 79 rpm during spraying. All coatings were sprayed using a Diamond Jet™2600 gun with a Diamond Jet™7-8 nozzle moving vertically during spraying. H_2 was used as the fuel gas and was mixed with O_2 at a ratio of 0.3. The flame was used to pre-heat the substrates and subsequently the powder was fed into the flame at a rate of 21–22 g/min. Ten strokes with the gun were made at a distance of 230 mm to deposit the coatings.

Table 1 Powder size distributions

Powder	d10 (μm)	d50 (μm)	d90 (μm)
XSmall (XS)	6.23	30.4	56.5
Small (S)	20.1	38.2	64.7
Medium (M)	24.6	47.3	81.5
Large (L)	33.7	56.3	88.0

10% of the grains are smaller than d10 and 10% are larger than d90. d50 is the average size of the powder

In-flight characterization of the sprayed particles, such as mean particle velocity and temperature, was made with an optical sensing device, Tecnar DPV-2000 [13]. This instrument is equipped with an infrared pyrometer and a dual optical slit, which has a width of 210 μm. The measurement volume was 0.7 mm^3 and the particle velocity and temperature were obtained with a precision of 0.5% and 3%, respectively. Measurements were performed with the S powder at high, medium and low gas flow rates at a distance of 230 mm from the gun nozzle. A mean value was calculated from *x*–*y* measurements.

Microstructural analysis

The coatings have been characterized using various techniques. X-ray diffraction (XRD) has been used to obtain the overall phase composition of the sprayed coatings. Analyses were performed in a Philips X'Pert MRD X-ray diffractometer in Bragg–Brentano geometry using a point-focus Cu Kα source and a plate collimator detector operated at 45 kV and 40 mA.

An average elemental composition of the films was measured employing Time-of-Flight Elastic Recoil Detection Analysis (ToF-ERDA) at the Uppsala Tandem Laboratory using 40 MeV $^{127}I^{9+}$ projectile ions at 22.5° incident angle and a detector placed at a recoil scattering angle of 45°. ERDA was primarily used to acquire the oxygen content in the coatings.

To obtain a good overview of the microstructure, with topographical and elemental contrast on the nanometer scale, scanning electron microscopy (SEM) was applied. A Leo Ultra 55 field emission gun (FEG) SEM and an FEI Quanta 200 Environmental FEGSEM were used. Both instruments are equipped with Oxford Inca energy dispersive spectrometers (EDS), which give chemical information at a resolution of about 1 μm. Prior to analyses in the SEM, the samples were cut in a high-speed saw and both cross-section and top view samples were polished using three grades of diamond slurry.

To image the samples at a higher magnification and to achieve higher resolution during chemical analyses transmission electron microscopy (TEM) was used. All TEM work was performed on a Philips CM200 FEG TEM equipped with an EDS spectrometer and a Gatan energy selective imaging filter (GIF). So-called Energy Filtering TEM (EFTEM) has been used to map 10 eV energy intervals in the low energy loss region and to make elemental maps. Elemental mapping was done with the jump ratio technique. In this technique, the image obtained using an energy window after the peak edge of the specific element is divided by the image acquired using the energy window before the peak edge [14]. This technique offers several advantages such as high signal-to-noise ratio, low

levels of diffraction contrast and under certain circumstances, it can be the only viable option, e.g. in the low-loss region with overlapping edges [15, 16]. The energy-loss spectrum edges used were, Al–K, Ti–$L_{2,3}$, C–K and O–K. To prepare electron transparent specimens for the TEM, the in situ lift-out technique [17, 18] was performed using a focused ion beam (FIB)-SEM FEI Strata 235 dual beam workstation. This instrument was also used for imaging by detection of secondary electrons created by impinging ions.

Pore analysis was performed using the software ImageJ. A series of gray level thresholds were selected, and for each created binary image the area density was calculated. To choose an appropriate threshold representing pores, the threshold was selected as the value where the gradient of the area density versus threshold curve increased considerably.

Results and discussion

Microstructure of the coatings

All the investigated coatings are relatively dense, showing a layered splat structure. This microstructure is typical for thermal spray coatings. Figure 1 shows an example of a cross-sectional SEM image of the coating made with the XS powder at the high gas flow. This micrograph is obtained using backscattered electrons and therefore, contrast variations indicate the presence of different phases. The brightest regions correspond to the heaviest phases and the darkest contrast comes from pores and pullouts caused by polishing. From the area density of such dark contrast, we find that the different coatings contain 2–8% porosity, assuming no pullouts. However, using other polishing techniques, with rougher finish, the obtained porosity value was less than 1%. It is therefore concluded that the majority of the dark contrast in Fig. 1 results from too harsh polishing and suggests poor cohesion in the coatings. This is fortified by the inability to measure porosity with the BET (Brunauer, Emmett and Teller) method [19] where it falls below the detection limit for this technique.

Even though the coatings are sprayed with Ti_2AlC powder, that contains a minor fraction of Ti_3AlC_2 [10], the X-ray diffractogram in Fig. 2 shows strongest intensities for polycrystalline TiC. There are also peaks corresponding to Ti_2AlC, Ti_3AlC_2 and titanium aluminides (Ti_xAl_y). The distribution of the phases Ti_2AlC, TiC and Ti_xAl_y is demonstrated using SEM and TEM. Figure 3 shows more details of the microstructure, of the sample in Figs. 1 and 2,

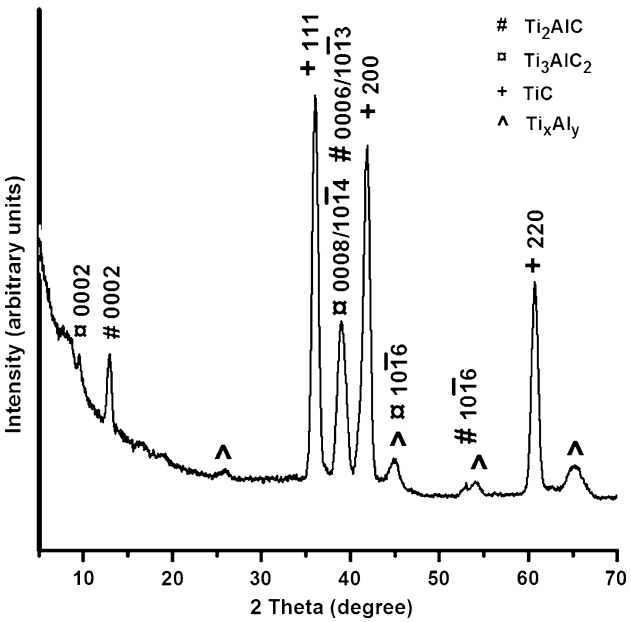

Fig. 2 X-ray diffractogram of the coating sprayed with the XS powder at the high gas flow. The presence of Ti_2AlC, Ti_3AlC_2, TiC and Al_xTi_y is clearly visible

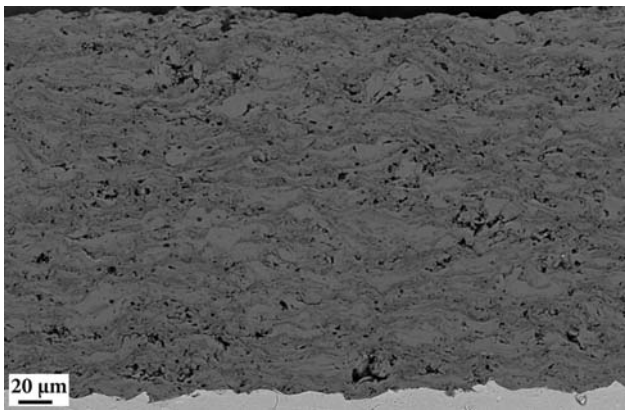

Fig. 1 Low magnification backscattered electron SEM micrograph showing a cross-section of a typical HVOF sprayed Ti_2AlC coating made with the XS powder at the high gas flow

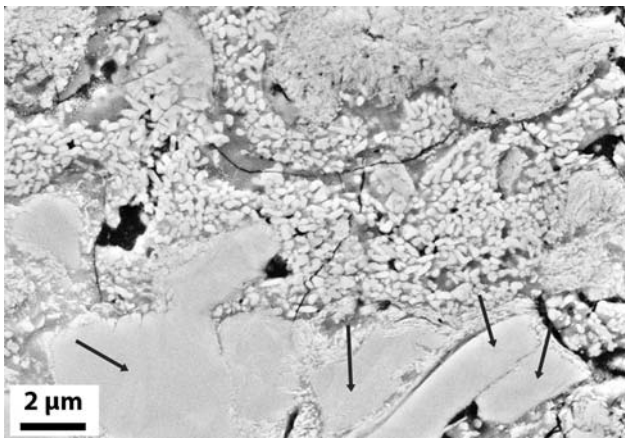

Fig. 3 Top view secondary electron SEM image showing details of the complex morphology of the coating made with the XS powder at the high gas flow. *Arrows* indicate unmelted powder grains

obtained by SEM. This micrograph reveals two types of regions in the coating. One, containing relatively large grains (indicated by arrows in Fig. 3) the other consisting of very small grains. Each of the large grains is smaller than about 15 μm while the size of the small grains is less than 500 nm. Furthermore, the small grains are embedded in a dark-gray appearing phase that will be referred to as the matrix phase in the following text.

Most of the large grains have been identified as Ti_2AlC but some large TiC grains have also been found. Figure 4 gives further insight into the chemistry of the coatings. A SEM backscattered electron image of a typical region of the coating with a large Ti_2AlC grain in the centre is shown in Fig. 4a. EDS elemental maps of this region are shown in Fig. 4b–e, while Fig. 4f is a phase map of the area. Each phase in the phase map corresponds to areas with the same average composition. The maps together with point analyses reveal that thin aluminum-rich zones surround the large Ti_2AlC grain as well as the small-grained regions. These zones also contain titanium, carbon and some oxygen. Outside the Al-rich zones are areas with more incorporated oxygen and also a few completely oxidized grains. The compositions of the oxidized zones have a Ti to Al ratio in the range of 0.5–2.5. The overall O content in this coating is 25 at.% as determined by ToF-ERDA. This is significantly higher than that in the bulk material used for making the powder (∼2 at.%) and can obviously be explained by oxidation during the HVOF process.

The spatial resolution in compositional analysis in SEM is not sufficient for detailed investigations of regions containing small grains. Therefore, to analyze the composition of the small grains and the matrix phase surrounding them, a combination of EFTEM and EDS in the TEM has been used. Figure 5 shows EFTEM images of a thin sample of the coating made with the XS powder at the high gas flow. Using the four elemental jump ratio images, showing high intensity signals for carbon and titanium in the small grains, the small grains were identified as TiC. EDS point analysis in the TEM confirms this result. It is also clear from the oxygen and aluminum jump ratio images, in Fig. 5, that there is aluminum oxide in the coating. The TiC grains are surrounded by a matrix of titanium aluminide. According to EFTEM and EDS analyses, the titanium aluminide does not have a fix composition throughout the coating; it varies with size and distribution of the adjacent TiC grains. This is demonstrated by the EFTEM image in Fig. 6, showing the existence of two differently appearing matrix phases with smaller grains embedded. The image is recorded at an energy of 15 eV, which coincides with the Al plasmon peak [20, 21]. This indicates that the area with brighter contrast is a phase containing more aluminum, which is confirmed by EDS analyses. The Ti to Al ratio is close to 0.8 while the dark contrast phase has a ratio around 1.5 according to EDS analyses. There can also be a varying amount of oxygen in the matrix phase. The variation in Ti_xAl_y stoichiometry is also supported by the XRD results

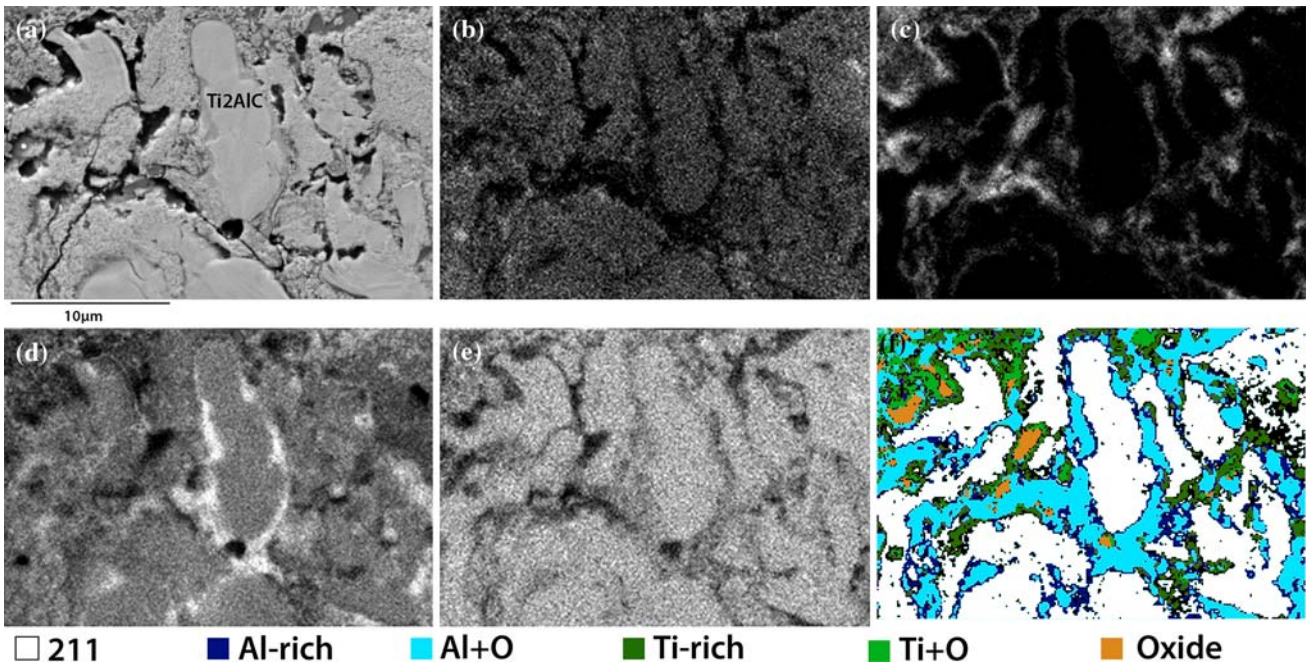

Fig. 4 EDS elemental distributions of the major elements present in the coating made with the XS powder at the high gas flow; **a** SEM micrograph, **b** C, **c** O, **d** Al, **e** Ti and **f** phase map. The legend refers to the relative amount of Ti and Al compared to the original 211 with a Ti to Al ratio of 2

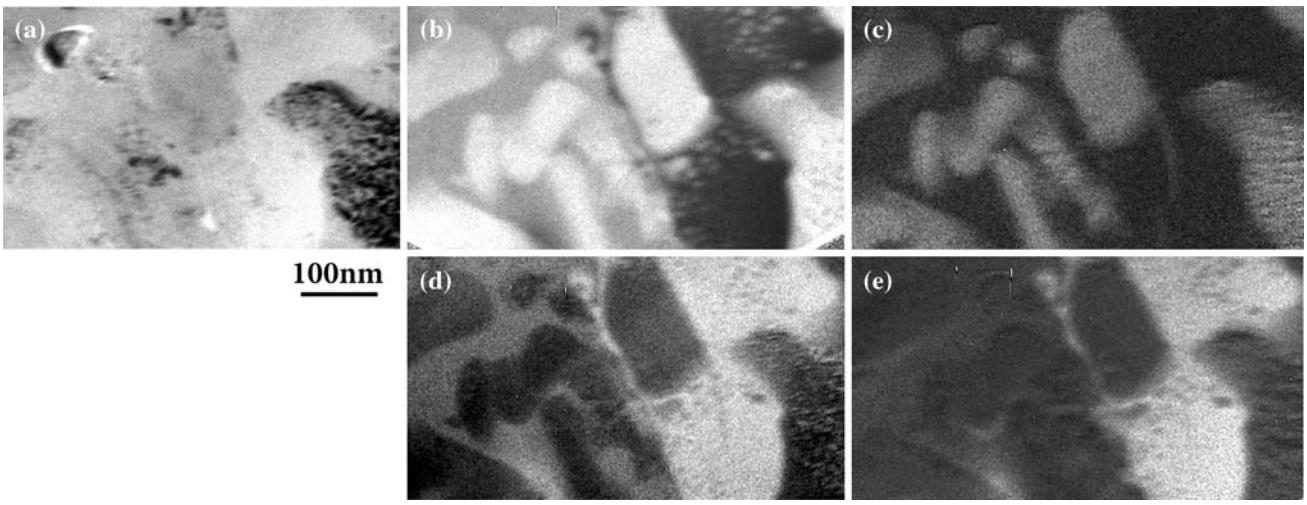

Fig. 5 Details in compositional variations by EFTEM; **a** zero loss, **b** Ti jump ratio, **c** C jump ratio, **d** Al jump ratio and **e** O jump ratio. The coating is made with the XS powder at the high gas flow

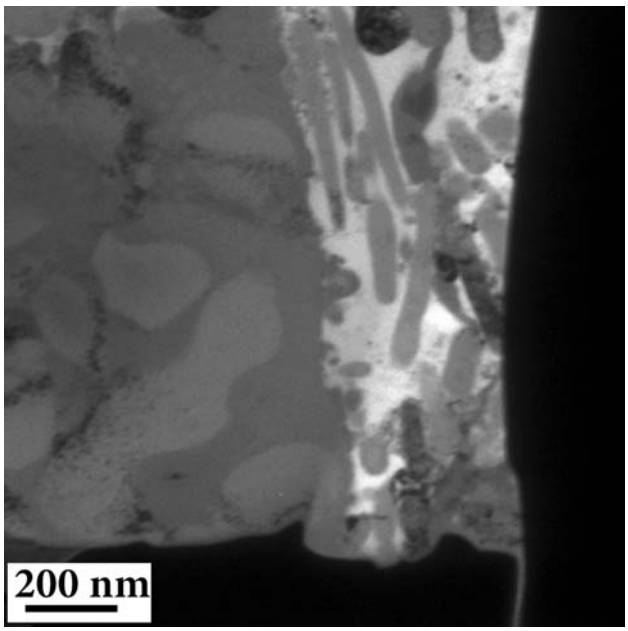

Fig. 6 EFTEM image showing the presence of small grains embedded in two different matrix phases. The image is recorded at an energy of 15 eV, and the coating is made with the XS powder at the high gas flow

where the broad titanium aluminide peaks originates from overlapping diffractions from both Ti- and Al-rich phases. Looking at the Ti–Al phase diagram [22], there are several titanium aluminides in the interval found from EDS analysis, such as Ti_3Al, TiAl and $TiAl_2$.

Based on the so far presented results, it is clear that during the spray process the Ti_2AlC powder decomposes. Different stages of this gradual decomposition of the once solid Ti_2AlC grains are depicted in the SEM micrographs in Fig. 7. First, only a thin rim surrounding the grain is decomposed (Fig. 7a). Then more and more of the grain is broken up into smaller grains (Fig. 7b, c). The microstructure of the obtained coating is built up of layers of unmelted and partially melted, decomposed Ti_2AlC grains embedded in a mixture of Ti_xAl_y and TiC grains. It appears that during the spraying process, the outer part of the original grains melt or partially melt and oxidize while the interior of the grains start to suffer from outward diffusion of aluminum. This statement is supported by Fig. 4 in which the Ti_2AlC grain seen in the middle of the image corresponds to the unmelted core of the powder grains while the alleged outward diffusion of Al is indicated by an Al rich phase surrounding this grain. The decomposition of Ti_2AlC by Al outward diffusion is also supported by the fact that in this structure the Ti–Al bonding is weaker than that between Ti and C [6] and that the decomposition of closely related structure of Ti_3AlC_2 is triggered by deintercalation of Al [23]. It is believed that this diffusion occurs preferentially along the basal planes, since these planes offer the most open diffusion paths [23]. The observed presence of small TiC grains embedded in titanium aluminides that are adjacent to the unmelted core of the Ti_2AlC grains in Fig. 4 can be explained by two different mechanisms: (1) transformation of Al deficient Ti_2AlC during spraying to cubic TiC via Ti_3AlC_2. To preserve the mass balance, this transformation should also be assisted by the formation of Ti_xAl_y phases; (2) formation of TiC and Ti_xAl_y during fast solidification (cooling rate about 10^6 °C/s [11]) of the molten parts of the grains upon impact on the substrate. It is most probable that during solidification these phases crystallize easier than Ti_2AlC

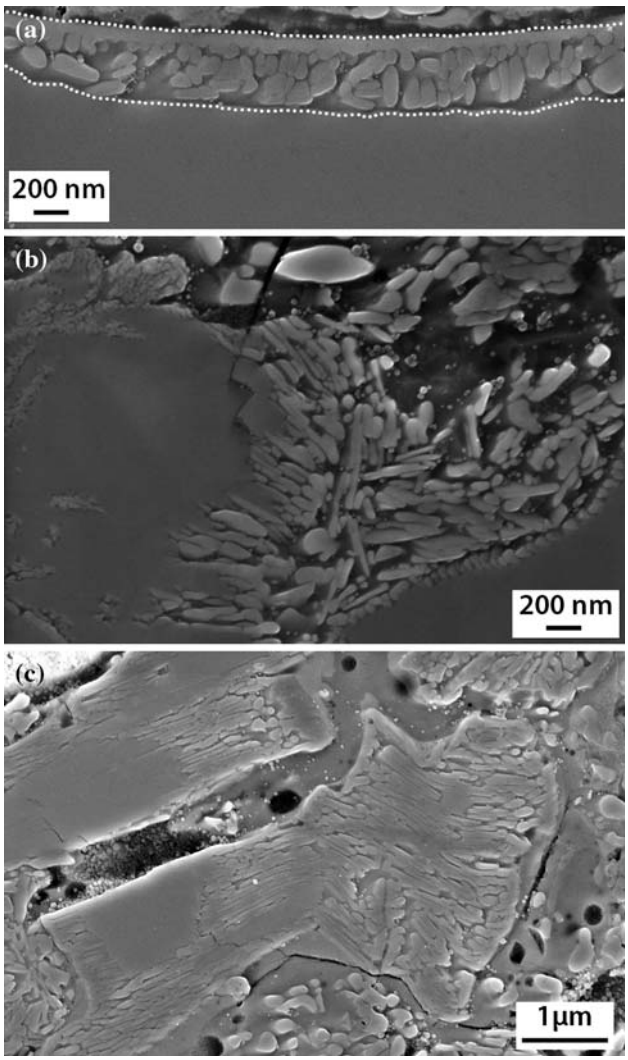

Fig. 7 Three SEM micrographs, of the coating made with the XS powder at the high gas flow, showing different stages of decomposition. The *white dotted lines* in **a** delineate the decomposed rim surrounding the MAX phase grain. A more advanced decomposition is seen in **b** and **c**

because they do not require a complex rearrangement of the elements. Another process that definitely takes place is oxidation since oxidized zones, i.e. the outer zones of the powder grains that have been in contact with air, surround the different regions. The presented reasoning also supports our previous model behind the phase transformation during coating formation [10].

Influence of fabrication parameters on coating microstructure

To obtain coatings containing high amount of Ti_2AlC, the transformation of Ti_2AlC to TiC and Ti_xAl_y must be minimized. However, it is also important to have some Ti_xAl_y in the coating, since it serves as a binder phase. Optimization of the coating composition can be achieved by tuning of the spray parameters. There are many factors controlling coating properties such as particle size, velocity and temperature, spray distance, flame characteristics, substrate temperature etc. [11]. In this study, powder size distribution and flame power, through gas flow rate, have been varied.

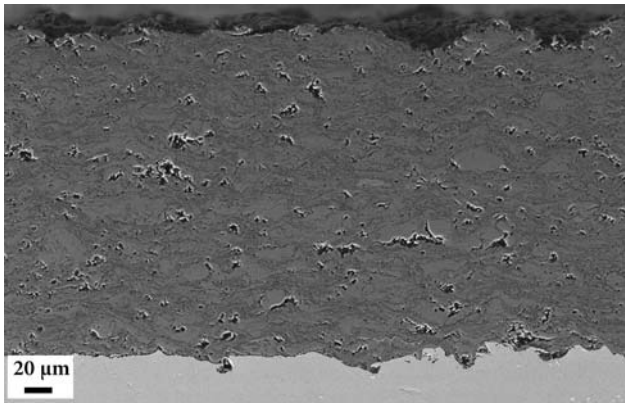

Fig. 8 SEM micrograph of a cross-section of the coating made with the XS powder at the medium gas flow

Table 2 Average thickness of the coatings in μm

Gas flow/Powder	XS	S	M	L
High	210	–	–	–
Medium	220	200	200	150
Low	–	120	100	≤50

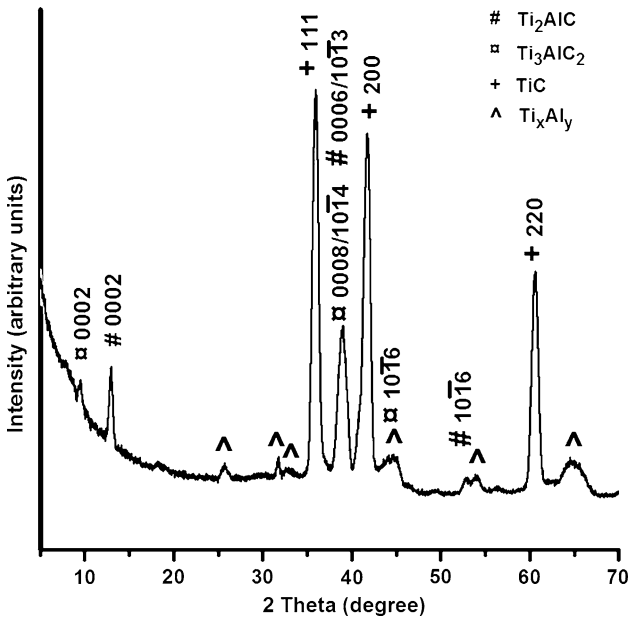

Fig. 9 X-ray diffractogram of the coating produced with the XS powder at medium gas flow

Influence of gas flow on microstructure

The microstructure of the two coatings made from the XS powder but with different gas flows are very similar, see Figs. 1 and 8. Figure 8 shows a cross-sectional SEM image of the coating sprayed with the XS powder at the medium gas flow. There are no delaminations in the coatings or at the interface, and their surfaces are smooth. Both coatings also have similar thickness, around 210 μm, see Table 2. Additionally, the X-ray diffractograms of the two coatings, Figs. 2 and 9, reveal that the two coatings have similar composition with a majority of TiC and Ti_2AlC, some Ti_xAl_y and small amounts of Ti_3AlC_2. Thus, for the XS powder the applied changes in total gas flow rate do not affect the microstructure of the coatings. This is not the case for the other powder types.

Figure 10 shows SEM cross-sectional micrographs of the six coatings produced at medium and low gas flows with the three different powders S, M and L, respectively. It is clear from these images that the coatings sprayed with the low gas flow (Fig. 10b, d f) are thinner than their counterparts sprayed at the medium gas flow (Fig. 10a, c, e). Furthermore, for the S and M powders, the coatings produced with the low gas flow contain more and larger unmelted grains compared to the medium gas flow coatings. Lower gas flow also yields an increase in the Ti_2AlC to TiC ratios, as shown in the X-ray diffractograms in Fig. 11a–d. For the L powder, lowering the gas flow will

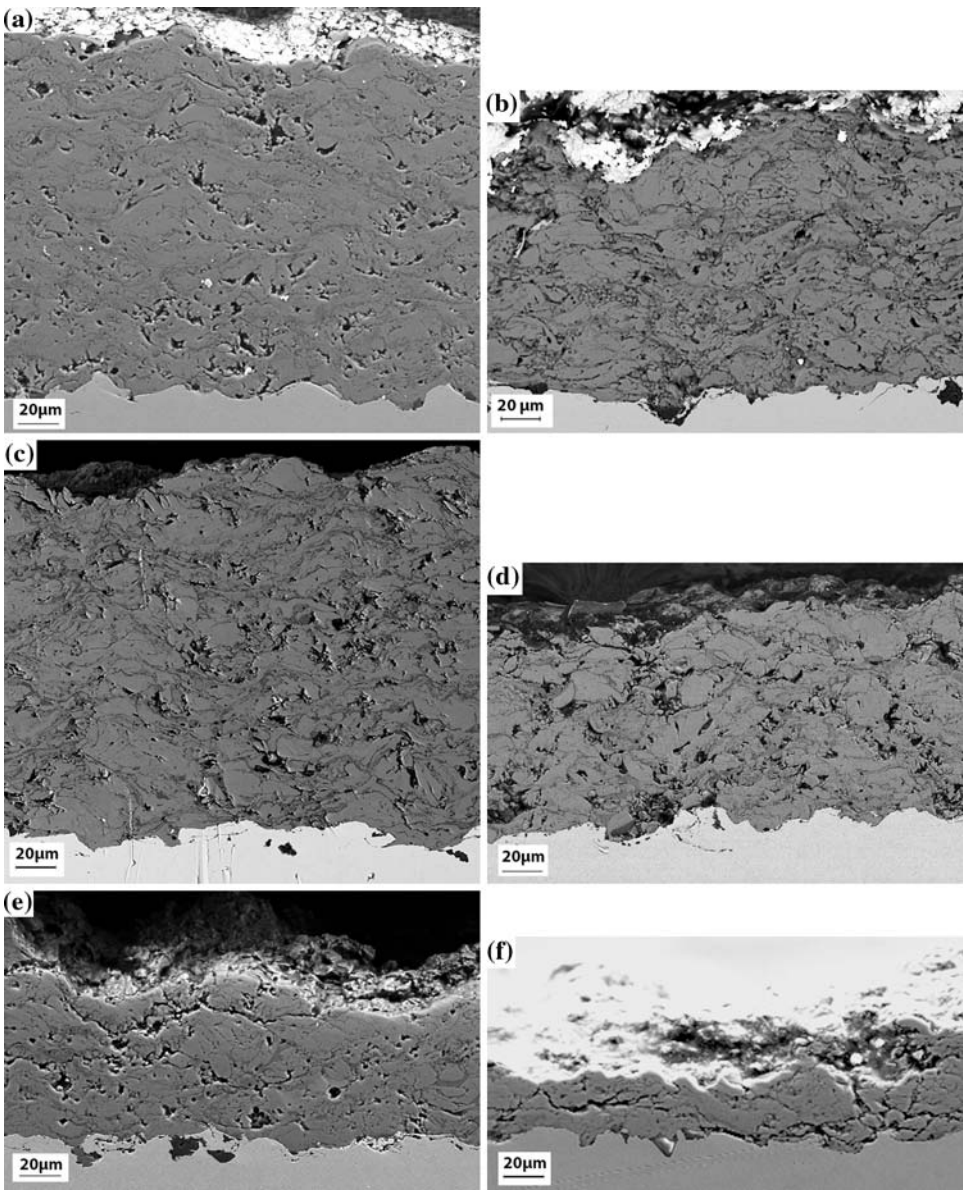

Fig. 10 SEM cross-sectional micrographs of the coatings made with powders S, M and L at medium and low gas flows. **a** S powder, medium gas flow, **b** S powder, low gas flow, **c** M powder, medium gas flow, **d** M powder, low gas flow, **e** L powder, medium gas flow and **f** L powder, low gas flow

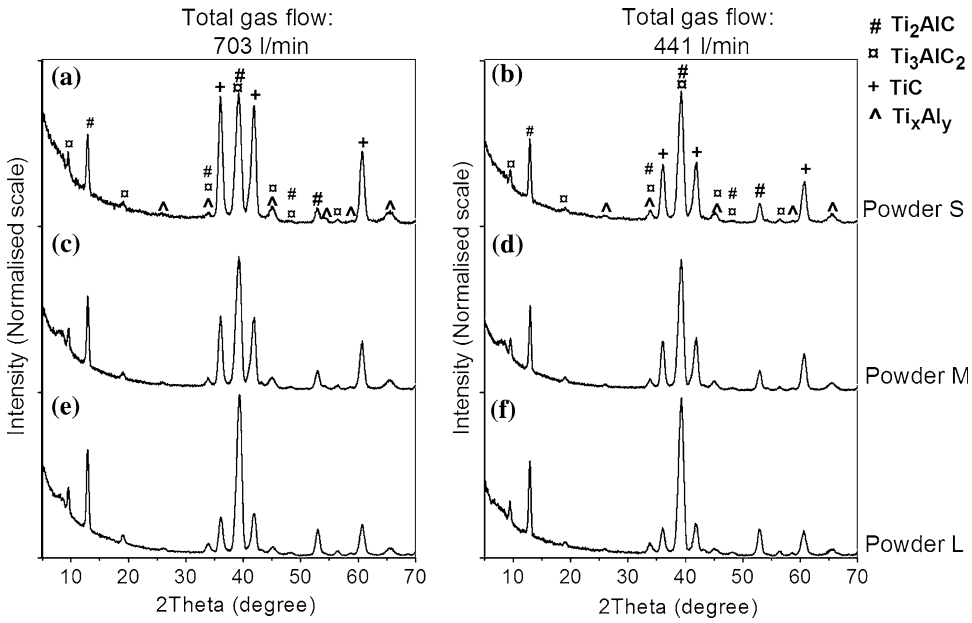

Fig. 11 X-ray diffractograms of coatings made with powders S, M and L at medium and low gas flows

also increase the amount of cracks and make the cracks larger, as shown in Fig. 10e, f. The amount of oxygen is, however, equal for low and medium gas flows. ToF-ERDA measurements for the coatings presented in Fig. 10a, b show an oxygen content of 15 and 14 at.%, respectively. This is a decrease of ~10 at.% compared to the coating sprayed with XS powder and high gas flow presented in Fig. 1.

Some differences in the microstructure due to changes in gas flow rates can be explained by the results from the DPV measurements presented in Table 3. In-flight particle temperatures and velocities were measured for powder S at all three gas flow rates. The large difference in velocity between medium and low gas flow rates changes the conditions for impact and solidification and thereby alters the adhesion of the coatings. Specifically, the particles are less likely to attain the critical kinetic energy needed to achieve deposition when the gas flow is lowered. Instead the incoming grains bounce off the substrate during spraying. Thus, the coatings sprayed at low gas flow rates are thinner.

The DPV measurements also show that the temperatures of the powder surface for all gas flow rates are in the same range, ~2100 °C, considering an accuracy of 3%. This is the melting temperature for Al_2O_3, which is most likely to form already on the surface of the sprayed particles. It is therefore believed that the emissivity used for temperature measurements reflects the temperature of the alumina layer on the surface rather than the temperature inside the powder. Furthermore, in this study the O_2/H_2 ratio is constant for all gas flow rates, and it is the oxygen to fuel gas ratio that determines the flame temperature. Thus, the flame temperature should be similar for all the spraying conditions. However, the power of the flame, which determines the thermal transfer, is proportional to the gas flow [24], and therefore the temperature of the inner parts of the powder grains can still be expected to vary. This explains why there is an increase in amount of Ti_2AlC for lower gas flows due to less decomposition of the powder.

Table 3 Results of the DPV measurements

Gas flow	Velocity (m/s)	Temperature (°C)
High	849 ± 24	2076 ± 27
Medium	719 ± 13	2111 ± 18
Low	503 ± 12	2113 ± 21

The in-flight velocity and surface temperature of the powder at three different gas flow rates are listed

Influence of powder size on microstructure

The present study shows that different powder size distributions will influence both coating cohesion and thickness. Since we are interested in coatings with a high amount of Ti_2AlC, the microstructural investigations were directed towards identification of phases present in the coatings and not towards quantification of porosity. However, as stated previously the dark contrast in the presented SEM micrographs is mainly from pullouts and can thus be used as an indicator of a quite weak cohesion in the coatings. At medium gas flow, the coating made from the finest powder (XS) contains fewer pullouts than the other three coatings sprayed with the S, M and L powders, see Figs. 8 and 10a, c, e. Both the S and M powders produce coatings with similar structures. While the coarsest powder (L) results in

a coating with cracks in the coating and at the interface, Fig. 10e. The L powder coating is also the thinnest of the four coatings, only 150 μm compared to at least 200 μm for the other coatings sprayed at medium gas flow, see Table 2. The same trend is observed for the coatings sprayed at the low gas flow. Changes in powder size distribution also affect the composition of the coatings, e.g. as noted previously the oxygen content decreased by ~10% between XS and S powder. A full quantification of the different phase fractions is complicated by the apparent crystallographic texture and crystal defects induced by the deposition process. We have nevertheless made a comparison between the crystalline MAX phases (including Ti_2AlC and Ti_3AlC_2) with TiC based on the XRD results. In Fig. 11 it is seen that the lowest MAX phase to TiC ratio is observed for the coating made with medium gas flow and the S powder. As the powder size increases, the amount of MAX phase compared to TiC doubles for the M powder and doubles again for the L powder. When making the same comparison for the low gas flow between powder S and M there is obviously not as dramatic change. However, the amount of MAX phase is three times higher for the L powder compared to the M powder. Thus, we observe that spraying with a larger powder size results in more MAX phase and that to increase the amount further, a low gas flow is preferred. This agrees well with the observed changes in microstructure; coatings made with larger powders consist of more and larger unmelted Ti_2AlC grains. This is illustrated in Fig. 12 showing FIB micrographs of the coatings produced at medium gas flow with S and L powders, respectively.

HVOF is both a thermal and kinetic process, and there is a critical energy needed to deposit the powder particles. The amount of energy transferred from the flame to the powder varies with the size of the powder, which influences both degree of melting and velocity. Changes in particle velocity in turn influence the impact energy. Higher energy leads to higher particle deformation upon impact, which results in coatings with better cohesion and higher density. The degree of melting also affects the impact as a higher thermal energy gives higher fluidity and plasticity of the powder upon impact, which decreases coating porosity.

The obtained results agree well with the above reasoning. The larger powder grains in the L powder attain lower kinetic and thermal energy than the smaller powders. This leads to a lower sticking coefficient, resulting in a thinner coating with poor cohesion. At the same time, the lower degree of melting results in more retained Ti_2AlC in the coatings produced with the L powder. Furthermore, it is clear that for the XS powder the thermal energy is above the critical level for all tested gas flows, which subsequently do not alter the coatings.

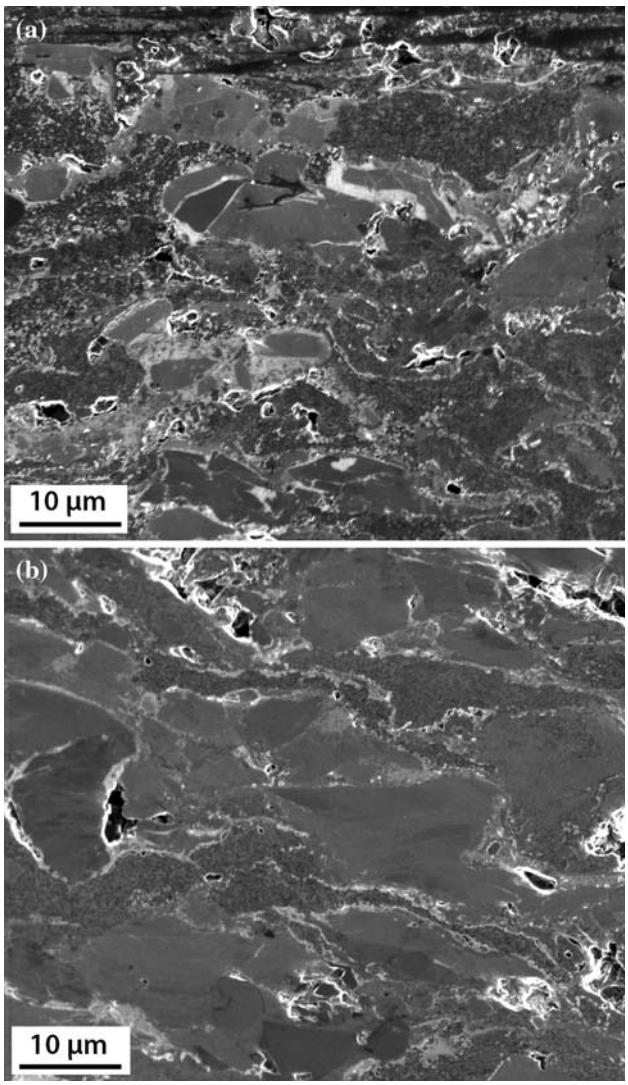

Fig. 12 FIB micrographs of coatings made at medium gas flow with **a** S and **b** L powder, respectively

Conclusions

Ti_2AlC coatings, made by HVOF spraying from Ti_2AlC powder, have a complex structure, both in terms of microstructure and composition. During the spraying process, parts of the Ti_2AlC powder transform to Ti_3AlC_2 and then to TiC and Ti_xAl_y due to an outward diffusion of Al. The resulting coating is composed of large, more than 10 μm, Ti_2AlC and TiC grains and very small TiC grains (<500 nm) embedded in titanium aluminide. The composition of the titanium aluminide is dependent on the local surrounding, i.e. the distribution of TiC grains. It is also observed that some oxidation of these phases takes place since oxygen rich zones surround the grains. The average oxygen content is inversely proportional to the powder size while the amount of retained Ti_2AlC can be adjusted with powder size and flame power. These factors also affect

thickness and cohesion of the coatings. Large powders form thinner coatings with higher amount of Ti_2AlC, but more susceptible to cracks compared to coatings made with small powders. The same applies for low flame power.

Acknowledgements Stefan Björklund at University West, Trollhättan, is acknowledged for his knowledge and support regarding thermal spray, and for handling the practicalities regarding the thermal spray sessions. Raymond Zakrisson, Volvo Aero Corporation, Trollhättan, is acknowledged for handling the spray equipment, and Jimmy Johansson, also at Volvo Aero Corporation, is acknowledged for his knowledge and handling of the DPV equipment. Jens Jensen at Thin Film Physics at Linköping University is acknowledged for knowledge and handling of the ERDA measurements. The Wallenberg foundation is acknowledged for funding the SEM, and the Swedish National Graduate School in Material Science is acknowledged for financing the project. LH, HH, and JF acknowledge support from the VINNEX Center FunMat.

References

1. Barsoum MW (2000) Prog Solid State Chem 28:201
2. Sundberg M, Malmqvist G, Magnusson A, El-Raghy T (2004) Ceram Int 30:1899
3. Byeon J, Liu J, Hopkins M, Fischer W, Garimella N, Park K, Brady M, Radovic M, El-Raghy T, Sohn Y (2007) Oxid Met 68:97
4. Wang X, Zhou Y (2003) Oxid Met 59:303
5. Zhou W, Mei B, Zhu J, Hong X (2005) Mater Lett 59:131
6. Wilhelmsson O, Palmquist J, Lewin E, Emmerlich J, Eklund P, Persson P, Högberg H, Li S, Ahuja R, Eriksson O, Hultman L, Jansson U (2006) J Cryst Growth 291:290
7. Rosén J, Ryves L, Persson POA, Bilek MMM (2007) J Appl Phys 101:056101
8. Mao Z, Ma J, Wang J, Sun B (2009) J Mater Sci 44:3265. doi: 10.007/s10853-00903438-3
9. Pasumarthi V, Chen Y, Bakshi SR, Agarwal A (2009) J Alloy Compd 484:113
10. Frodelius J, Sonestedt M, Björklund S, Palmquist JP, Stiller K, Högberg H, Hultman L (2008) Surf Coat Technol 202:5976
11. Davis J (2004) Handbook of thermal spray technology. ASM International, Ohio, USA
12. Kaufold RW, Rotolico AJ, Nerz J, Kushner BA (1991) In: Thermal spray research and applications: proceedings of the 3rd national thermal spray conference, Long Beach, California, May 1990, ASM International, pp 20–25
13. Mauer G, Vaßen R, Stöver D (2007) J Therm Spray Technol 16:414
14. Thomas PJ, Midgley PA (2002) Top Catal 21:109
15. Hofer F, Warbichler P, Grogger W (1995) Ultramicroscopy 59:15
16. Hofer F, Warbichler P, Grogger W, Lang O (1995) Micron 26:377
17. Liu F, Josefsson H, Svensson JE, Johansson LG, Halvarsson M (2005) Mater High Temp 22:521
18. Kothleitner G, Rogers M, Berendes A, Bock W, Kolbesen BO (2005) Appl Surf Sci 252:66
19. Brunauer S, Emmet PH, Teller E (1938) J Am Chem Soc 60:309
20. Wang ZL, Van Heerden D, Josell D, Shapiro AJ (1997) J Res Natl Inst Stand Technol 102:1
21. Williams DB, Carter CB (1996) Transmission electron microscopy. Plenum Press, New York
22. Raghavan V (2005) J Phase Equilib Diffus 26:171
23. Zhang J, Wang JY, Zhou YC (2007) Acta Mater 55:4381
24. Wigren J, Hansson M, Gougeon P, Moreau C (1996) In: Berndt CB (ed) Thermal spray: practical solutions for engineering problems. ASM International, Materials Park, Ohio, USA